Rotation-invariant colour texture classification through multilayer CCR

Francesco Bianconi,
Università degli Studi di Perugia
Dipartimento Ingegneria Industriale
Via G. Duranti, 67 - 06125 Perugia (ITALY)

Antonio Fernández, Elena González, Diego Caride, Ana Calviño
Universidad de Vigo
Escuela Técnica Superior de Ingeniería Industrial
Campus Universitario, 36310 Vigo (SPAIN)

Abstract

The *Coordinated Clusters Representation* (CCR) is a texture descriptor based on the probability of occurrence of elementary binary patterns (texels) defined over a square window. The CCR was originally proposed for binary textures, and it was later extended to grayscale texture images through global image thresholding. The required global binarization is a critical point of the method, since this preprocessing stage can wipe out textural information. Another important drawback of the original CCR model is its sensitivity against rotation.

In this paper we present a rotation invariant CCR-based model for colour textures which yields a twofold improvement over the grayscale CCR: first, the use of rotation-invariant texels makes the model insensitive against rotation; secondly, the new texture model benefits from colour information and does not need global thresholding. The basic idea of the method is to describe the textural and colour content of an image by splitting the original colour image into a stack of binary images, each one representing a colour of a predefined palette. The binary layers are characterized by the probability of occurrence of rotation invariant texels, and the overall feature vector is obtained by concatenating the histograms computed for each layer. In order to quantitatively assess our approach, we performed experiments over two datasets of colour texture images using five different colour spaces. The obtained results show robust invariance against rotation and a marked increase in classification accuracy with respect to grayscale versions of CCR and LBP.

Key words: colour texture classification, rotation invariance, CCR
PACS: 07.05.Pj, 42.30.Sy

1. Introduction

Texture analysis is a topic of intensive research activity with applications in many areas, such as medical imaging, remote sensing, surface inspection, image retrieval and others. Texture classification is a branch of texture analysis which results particularly well suited for the automatic grading of products such as ceramic tiles, marble and granite tiles, parquet slabs, etc. Based on this fact, an increasing attention from industry has recently emerged. Since in practical applications it is uncommon that texture images are captured under invariant viewing conditions, it is of great importance that texture classification be rotation, translation and scale invariant. Another issue in texture classification is about the role of colour. Even if many approaches to texture analysis have been proposed in the last three decades, in most cases such methods are applied to grayscale images. A comprehensive review of these techniques can be found in (Petrou and García-Sevilla, 2006). During the last years there has been a growing interest in extending traditional grayscale texture analysis to colour images. The approaches to deal with colour texture can be classified into three groups: *parallel*, *sequential* and *integrative* (Palm, 2004).

Parallel approaches consider texture and colour as separate phenomena. Colour analysis usually relies on the distribution of colours in an image, regardless of the spatial relationship between pixel intensity; texture analysis is based on the relative variation of the intensity of neighbouring pixels, regardless of their colour. The approach proposed by

Drimbarean and Whelan (Drimbarean and Whelan, 2001) belongs to this group. In this work the authors first convert the original RGB images into HSI, CIE XYZ, YIQ and CIELAB, and then extract texture features from the intensity channel (through Discrete Cosine Transform, Gabor filters and co-occurrence matrices) and pure chrominance features from the colour channels. In a similar way Hiremath et al. (Hiremath et al., 2006) work with the HSV and YCbCr colour spaces and extract wavelet features from the intensity channel and first order statistical features from the chrominance channels.

In sequential approaches the first step consists in applying a colour indexing method to the original colour images. As a result we obtain indexed images that can be processed as grayscale textures. In this framework the co-occurrence matrix has received a great deal of attention, due to its straightforward extension to indexed images (Arvis et al., 2004; Van den Broek and Rikxoort, 2004; Huang et al., 1997; Sertel et al., 2007; Singh et al., 2002). Sometimes this method is referred to as the *colour correlogram* (Hauta-Kasari et al., 1996), since it represents the probability of occurrence of the same colour in pairs of pixels at a given distance. Other texture descriptors have been used as well. In (Bianconi et al., 2007) the authors use three different colour indexing methods and three different texture features, resulting in nine independent classifiers which are combined together through diverse fusion schemes.

Integrative models are based on the spatial relationship of pixels. These approaches can be further subdivided into *single-band* if data are considered separately from each channel, or *multiple-band* if two or more channels are considered jointly. In the first group we can include the colour constant colour indexing of (Funt and Finlayson, 1995), the generalized co-occurrence matrix (Arvis et al., 2004) and a number of methods where classical grayscale texture descriptors are applied to each colour channel separately (Chindaro et al., 2005; Hiremath et al., 2006; Lepistö et al., 2005; Manthalkar et al., 2002; Paschos, 2001). Multiple-band approaches have also been obtained as extensions of classical grayscale texture descriptors, such as wavelets (Van de Wouver et al., 2003a), Gabor filters (Jain and Healey, 1998), co-occurrence matrices (Palm, 2004), Local Binary Patterns (Pietikäinen et al., 2002) and Markov Random Fields (Panjwani and Healey, 1995).

The aim of this work is to present a rotationally invariant descriptor for colour textures. Our approach is based on the *Coordinated Clusters Representation* (*CCR*) as texture descriptor. Herein we present a twofold improvement of this texture model: on the one hand, we obtain a rotation-invariant operator by clustering the 512 possible binary patterns of the original CCR into groups of rotationally equivalent patterns; on the other hand, we extend the model to colour texture by colour quantization, through which indexed images can be obtained from the original colour images. The basic idea of the method is that an indexed image can be viewed as a stack of binary images (layers). This makes it possible to apply the CCR operator to each layer. For this reason we refer to this approach as the *multilayer CCR*.

The remainder of the paper is organized as follows. In section 2 we give a detailed description of the method; in section 3 we discuss about colour spaces and their possible effects on classification; the experimental activity is presented in section 4 followed by results (section 5) and conclusions (section 6).

2. Description of the method

The method presented here relies on two buliding blocks: a rotation invariant-version of the CCR and a multilayer version for colour textures. Before describing in detail these two ideas (secs. 2.1 and 2.2) and how they are combined to give rotation-invariant multilayer features (sec. 2.3), we briefly recall the Coordinated Clusters Representation.

The CCR was originally intended for binary textures (Kurmyshev and Cervantes, 1996). In this model the feature vector is the histogram of occurrence of the possible binary patterns (*texels*) that can be defined in a square window. The dimension of these elementary patterns is usually set to 3x3 pixels, since this size provides good discriminative power at a reasonable cost in terms of both computing speed and memory consumption. In this case, the feature vector -denoted by $CCR_{3\times3}$- has 2^9 components. The procedure to assign a $CCR_{3\times3}$ code to a texel is outlined in fig. 1. Note that the arrangement of the weighting mask is arbitrary. A different arrangement of the weighting factors would only result in a different coding of the patterns. This model was later extended to grayscale texture images through global image thresholding. The binarization threshold must be selected judiciously in order to preserve textural information. Two methods have been proposed so far: *fuzzy C-means clustering* (Sánchez-Yáñez et al., 2003a) and *isoentropic partition* (Bianconi et al., 2007). Both methods are based on the gray-level histogram of the original image. Further extensions to colour images were based on computing chromatic and textural features separately and on combining them together through some fusion scheme (Kurmyshev and Sánchez-Yañez, 2005). The CCR is not invariant against rotation, and no rotation-invariant version has been published so far.

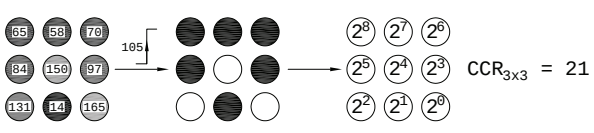

Fig. 1. Basic version of the CCR ($CCR_{3\times3}$). From left to right: original grayscale window, binary pattern after thresholding, weighting mask and $CCR_{3\times3}$ code.

2.1. *Rotationally invariant CCR operators*

Rotation-invariant CCR features can be obtained following an approach similar to the one proposed for the $LBP_{3\times3}$ operator (Ojala et al., 2002a), a related model in which the value of the central pixel of the 3x3 window is used for thresholding, resulting in 2^8 possible patterns. The first step consists in replacing the squared neighbourhood of the $CCR_{3\times3}$ by a circular one (Fig. 2). The gray-level values of the pixels that are not placed exactly on pixels positions are estimated through bilinear interpolation. We refer to this arrangement as the $CCR_{8,1}$.

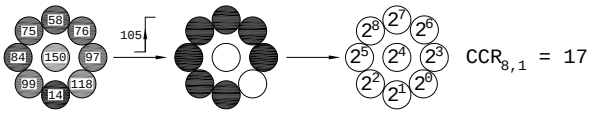

Fig. 2. Circularly symmetric version of the CCR ($CCR_{8,1}$). From left to right: original grayscale window, binary texel after thresholding, weighting mask and $\text{CCR}_{8,1}$ code.

The rotation invariant CCR operator, denoted by $CCR^{ri}_{8,1}$, is obtained by clustering all the patterns that are rotated version of the same pattern. This operation reduces the number of possible texels, and thus the dimension of the feature space from 512 to 72. Fig. 3 shows an example of this: the pattern coded 494 is represented together with its rotationally equivalent versions (namely texels 17, 24, 80, 144, 272, 48, 20 and 18). Rotationally equivalent patterns are assigned the same index.

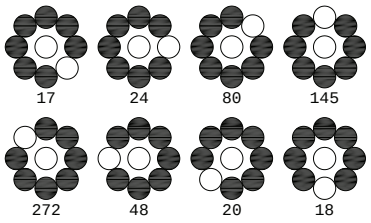

Fig. 3. Sample of rotationally equivalent patterns.

A further reduction in the dimension of the feature space can be obtained by taking into account the so called *uniform patterns* (Ojala et al., 2002a), that are patterns where the number of transitions in the eight peripheral pixels is at most two, regardless of the value of the central pixel. This gives 18 possible uniform texels, as shown in fig. 4. Following the implementation proposed in (Ojala et al., 2002a), the 19^{th} bin of the histogram accounts for all the remaining non-uniform patterns. We refer to this feature space as the $CCR^{riu2}_{8,1}$.

2.2. *Multilayer CCR*

The basic idea behind the multilayer CCR is that, given a set of representative colours (*palette*), a colour pattern (such as, for instance, a 3x3 window) can be represented

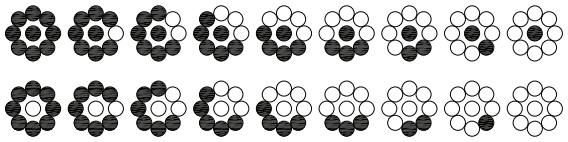

Fig. 4. The 18 possible uniform patterns of the $CCR^{riu2}_{8,1}$ feature space.

through a stack of binary patterns, one for each representative colour. Colour texture description through a stack of binary images obtained by colour indexing has been previously reported in (Song et al., 1996; Boukovalas et al., 1998). In these works texture is modelled by extracting morphological features from the binary layers. Herein we also perform a colour indexing pre processing stage to build a stack of binary images, but we characterize each binary layer by the frequency of occurrence of rotation invariant elementary texture patterns. In order to ensure meaningful comparison among different colour texture images, the set of representative colours have to be image-independent. To this end we adopted *uniform quantization* of the colour space: n samples are taken on each axis of the colour space, resulting in a palette of $N = n^3$ colours. Provided that the original colour images are given in the RGB space, we considered a good practice to do uniform quantization in this space. Figure 5 shows the resulting palettes with 8, 27 and 64 levels. We used the same palette for the RGB and sRGB spaces (a description of the colour spaces used in this work is given in sec. 3). When other colour spaces are used, the palette is converted to the new colour space through the transforms described in section 3.2. Once the palette has been computed, each pixel of a 3x3 colour neighbourhood is assigned the index of the nearest colour of the palette (herein we used the euclidean distance to determine the nearest colour). Afterwards the neighbourhood is split into a set of N binary layers, each layer corresponding to one of the N colours of the palette, with the convention that a pixel in the layer $l \in \{1, 2, ..., N\}$ takes value 1 if its colour index is l, and 0 otherwise. This results in a set of binary patterns (of the type of fig. 3), one for each layer. Now each binary pattern can be characterized through a proper binary texture descriptor, such as the CCR. Sequential scanning of the original image gives rise to N pattern distributions (histograms), one for each layer. The feature vector is formed by concatenating the histogram of each layer.

2.3. *Rotation-invariant multilayer features*

The basic ideas presented in the two previus sections can be combined together to obtain rotationally invariant features for colour textures. The entire process can be summarized as follows (see fig. 6): 1) establishment of an image-independent colour palette; 2) replacement of each square neighbourhood by a circular one; 3) colour indexing; 4) subdivision in binary layers; 5) calculation of the CCR code of

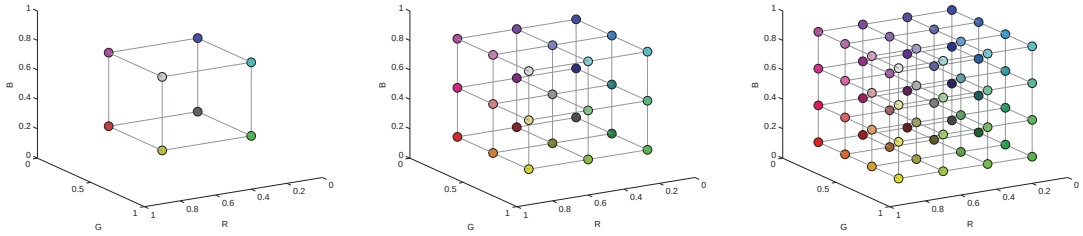

Fig. 5. Uniform quantization of the RGB and sRGB colour spaces with 8, 27 and 64 levels.

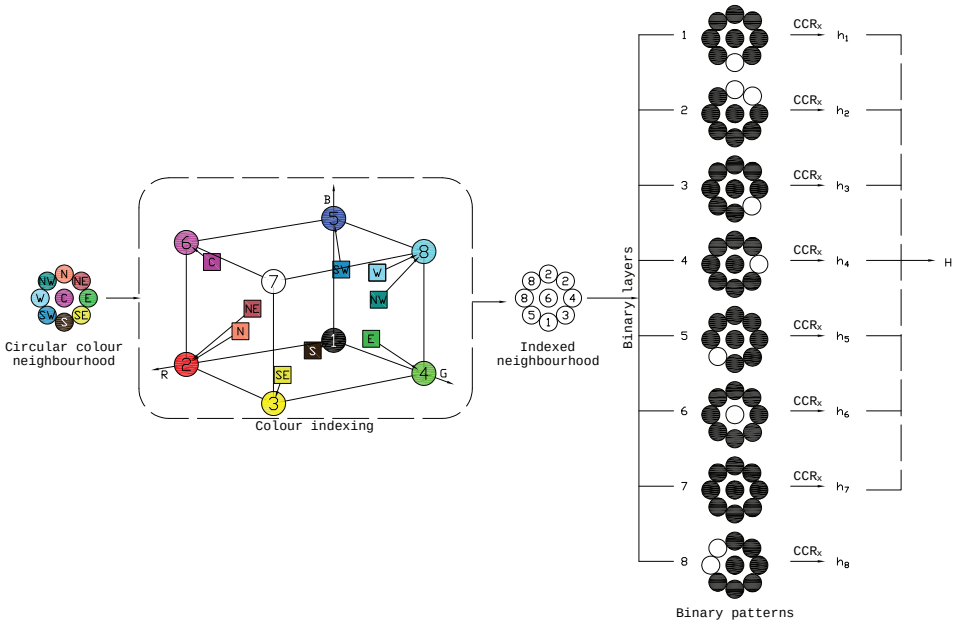

Fig. 6. Procedure to compute the multilayer CCR. Each colour pixel of the circular neighbourhood is assigned an index of a predefined palette composed of N colours (in this case $N = 8$). Cardinal points are used in the figure to indicate the position of the colours of each pixel of the circular neighbourhood in the colour space (RGB in this case).

the resulting binary patterns in each layer; 6) calculation of the CCR histogram of each layer; 7) concatenation of the resulting CCR histograms. It is worth noting that being the elements of the binary patterns mutually exclusive (if one pixel is 1 in one layer the pixels in the same position in the other layers are 0 by definition), only $(N-1)$ out of N binary patterns are independent, and thus $(N-1)$ layers suffice to describe the colour texture [1]. Any of the above described rotation-invariant CCR operators can be applied to the first $(N-1)$ binary layer, giving $(N-1)$ codes, one for each binary pattern. The feature vector H of the colour texture is obtained by concatenating the histograms of each layer: $H = [h_1\ h_2\ \cdots\ h_{N-1}]$, where h_l is the CCR histogram of the l-th layer. We refer to the multilayer CCR as $ML\_$ followed by the acronym of one of the three operators described in section 2.1. The resulting feature spaces are summarized in table 1.

Table 1
Characteristics of the feature spaces. N indicates the number of colours of the palette.

Feature space	Dimension	Colour	Rotation-invariance
$CCR_{3\times3}$	512	no	no
$CCR^{ri}_{8,1}$	72	no	yes
$CCR^{riu2}_{8,1}$	19	no	yes
$LBP_{3\times3}$	256	no	no
$LBP^{ri}_{8,1}$	36	no	yes
$LBP^{riu2}_{8,1}$	10	no	yes
$ML\_CCR_{3\times3}$	$(N-1)\times512$	yes	no
$ML\_CCR^{ri}_{8,1}$	$(N-1)\times76$	yes	yes
$ML\_CCR^{riu2}_{8,1}$	$(N-1)\times19$	yes	yes

[1] Without loss of generality in our implementation we discard the N-th level.

3. Colour spaces

The effect of different colour spaces in colour texture classification is still subject of controversial debate in the computer vision community. A brief review of related research shows that a general consensus on whether there is an optimal colour space or not has not been achieved yet. In fact, different authors have drawn contradictory conclusions from their experiments. Paschos found that HSV performs best, followed by CIELAB and RGB (Paschos, 2001). Similarly Van den Broek and Van Rikxoort showed that in their results the HSV space outperforms the RGB (Van den Broek and Rikxoort, 2004). Nevertheless Drimbarean and Whelan drew the conclusion that none of the colour spaces considered in their comparative experiment (RGB, HSV, YIQ, CIE XYZ and CIELAB) proved sufficiently superior (Drimbarean and Whelan, 2001). The same conclusion comes out from the work of Mäenpää and Pietikäinen, where the RGB, HSV, $I_1I_2I_3$ and CIELAB colour spaces are considered (Mäenpää and Pietikäinen, 2004).

3.1. *Device-dependent vs. device-independent colour spaces*

Colour spaces can be *device-dependent* or *device-independent*. A device-dependent colour space is a colour space where the resultant colour depends on the equipment and the set-up used to produce it. On the other hand a device-independent colour space is a colour model that does not depend on any specific device, but rather on the human vision system.

We considered in this work two device-dependent spaces (RGB and HSV) and three device-independent spaces (sRGB, sHSV and Lab). Herein we recall the basic differences between these spaces. Interested readers are addressed to specific books on colour science (Kang, 2006; Wyszecki and Styles, 1982) for an in-depth explanation.

In most cases the output of digital colour devices is given in the RGB space. In this space colours are defined within a unit cube through the additive colour-mixing model. A potential drawback of the RGB space in colour texture classification is that it is not perceptually uniform, and hence difference between colours in the RGB space does not correlate with human perception of colour difference. The HSV (Hue-Saturation-Value) is a modification of the RGB space. The HSV space can be represented through a hexcone where the vertical axis (V) indicates the darkness of the colour, the orthogonal distance to this axis is the saturation (S) and the angle around the vertical axis is the hue (H). Potential advantages of the HSV colour space are that it is more related to the human visual system than the RGB and that it is approximately perceptually uniform.

The basic device-independent colour space is the CIE XYZ. This system relies on three colour-matching functions, also referred to as the *standard observer*, related to the red, green and blue cones of the eye. A device-independent colour space can be considered as any space

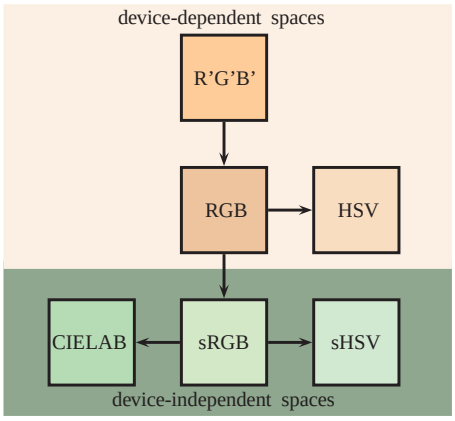

Fig. 7. Colour spaces and colour conversion pipeline

which has a one-to-one mapping (expressed through explicit mathematical equations) onto the CIE XYZ colour space (Vhrel and Trussell, 1998). The CIELAB can be computed via simple formulas from the XYZ space, and it is more perceptually uniform than XYZ. The three coordinates of CIELAB represent the lightness of the colour (L^*), its position between red/magenta and green (a^*), and its position between yellow and blue (b^*). The sRGB colour space is a colorimetric RGB specification based on the average performance of personal computer displays. It has received increasing attention since it has been adopted as the default colour space for the internet (Kang, 2006).

Changing from a device-dependent colour space to a device-independent one, requires estimating the relationship between the device-specific space and at least one device-independent space. This process is usually referred to as *colour calibration*, and diverse mathematical models have been proposed for it (Vhrel and Trussell, 1998).

3.2. *Transforms between the colour spaces*

Throughout this paper we assume that the original images are given in the RGB format. The colour conversion pipeline from the RGB space to the other spaces considered here is summarized in figure 7. Each transform is explained in detail here below.

$R'G'B' \rightarrow RGB$

In some cases, depending on the imaging device, RGB values may have a nonlinear luminance-to-signal relationship. This is usually known as *gamma correction* (or *gamma encoding*). We refer to gamma-corrected values as R'G'B'. If gamma correction is used, device-dependent linear RGB values have to be obtained from R'G'B' values through inverse gamma correction. For each channel the following luminance (x) to signal (y) relationship is usually assumed (Grana et al., 2004; Haeghen et al., 2000; Kang, 2006):

$$y = ax^{\gamma} + b \tag{1}$$

Converting the R'G'B' values into RGB requires estimating the values of a, b and γ of each channel an inverting equation 1. The procedure is described more in detail in section 4.3.1.

RGB → HSV

A simple relation exists between RGB and HSV (Kang, 2006):

$$V = max(R, G, B) \tag{2}$$

$$S = \begin{cases} 0 & : \quad V = 0 \\ 1 - min(R, G, B)/V & : \quad V > 0 \end{cases} \tag{3}$$

$$H = \begin{cases} 0 & : \quad S = 0 \\ 60(G - B)/SV & : \quad V = R \\ 60[2 + (B - R)]/SV & : \quad V = G \\ 60[4 + (R - G)]/SV & : \quad V = B \\ H + 360 & : \quad H < 0 \end{cases} \tag{4}$$

RGB → sRGB

In this work we adopted a linear model for colour calibration. This means that the transform can be expressed through equation 5 where the unknown a_{ij} values can be estimated through a calibration procedure, as detailed in section 4.3.2:

$$\begin{pmatrix} sR \\ sG \\ sB \end{pmatrix} = \begin{bmatrix} a_{11} & a_{12} & a_{13} \\ a_{21} & a_{22} & a_{23} \\ a_{31} & a_{32} & a_{33} \end{bmatrix} \begin{pmatrix} R \\ G \\ B \end{pmatrix} \tag{5}$$

sRGB → sHSV

This transform is the same as $RGB \rightarrow HSV$.

sRGB → CIELAB

This is a two-step procedure. First the sRGB values are converted into XYZ, and then from XYZ to $L^*a^*b^*$. A linear relation exists between sRGB and XYZ values (under illuminant D65) (Haeghen et al., 2000; Kang, 2006):

$$\begin{pmatrix} X \\ Y \\ Z \end{pmatrix} = 100 \begin{bmatrix} 0.4124 & 0.3576 & 0.1805 \\ 0.2126 & 0.7151 & 0.0721 \\ 0.0193 & 0.1192 & 0.9505 \end{bmatrix} \begin{pmatrix} sR \\ sG \\ sB \end{pmatrix} \tag{6}$$

In the above equation sRGB values are encoded within a range of [0,1]. XYZ values are then transformed into $L^*a^*b^*$:

$$\begin{pmatrix} L^* \\ a^* \\ b^* \end{pmatrix} = 100 \begin{bmatrix} 0 & 116 & 0 & -16 \\ 500 & -500 & 0 & 0 \\ 0 & 200 & -200 & 0 \end{bmatrix} \begin{pmatrix} f(X/X_n) \\ f(Y/Y_n) \\ f(Z/Z_n) \\ 1 \end{pmatrix} \tag{7}$$

where:

$$f(t) = \begin{cases} t^{1/3} & : \quad 1 \geq t \geq 0.008856 \\ 7.787t + (16/116) & : \quad 0 \leq t \leq 0.008856 > 0 \end{cases} \tag{8}$$

and X_n, Y_n and Z_n are the tristimulus values of the illuminant (D65 in this case).

4. Experimental set-up

In order to assess the performance of the feature spaces introduced in the foregoing sections, we carried out a set of texture classification experiments. To test the effectiveness of the multilayer CCR we compared its classification accuracy with the grayscale versions of both the CCR and the LBP. We used two texture datasets; in both of them the colour textures are hardware-rotated by the following angles: 0°, 5°, 10°, 15°, 30°, 45°, 60°, 75° and 90°. The textures which compose the datasets have been selected in compliance with the following criteria: a) *stationary* textures; b) planar or almost planar texture surfaces. Both criteria aim at avoiding possible source of bias in classification. According to the definition given in (Petrou and García-Sevilla, 2006), a stationary texture image contains a single type of texture and so its local statistical properties are the same everywhere in it. The use of stationary textures guarantees good texture sampling. Textures of non-planar surfaces can significantly change, due to the presence of shadows and highlights, as the surface rotates, with unpredictable effects on the results. The use of planar or almost planar texture samples reduces this problem.

4.1. *Datasets*

In the experimental activity we used two different datasets. The first one, herein referred to as the dataset A (fig. 8), is composed of 45 texture classes (one image for each class) from the OuTex library (Ojala et al., 2002b). The textures used here are a subset of the group *inca 100dpi*. The size of the original images is 746 x 538 pixels. As the texture surface rotates, only the central part of the image captures the same portion of the surface. For this reason we only retain the central part of the original images. If W and H are the width and height of the original image, the area to be retained is a centered square the dimension of which is $min(W, H)/\sqrt{2}$. This gives an image size of 380 x 380 pixels. Each image is subdivided into 16 non-overlapping sub-images, giving a database of 720 texture samples (16 for each class).

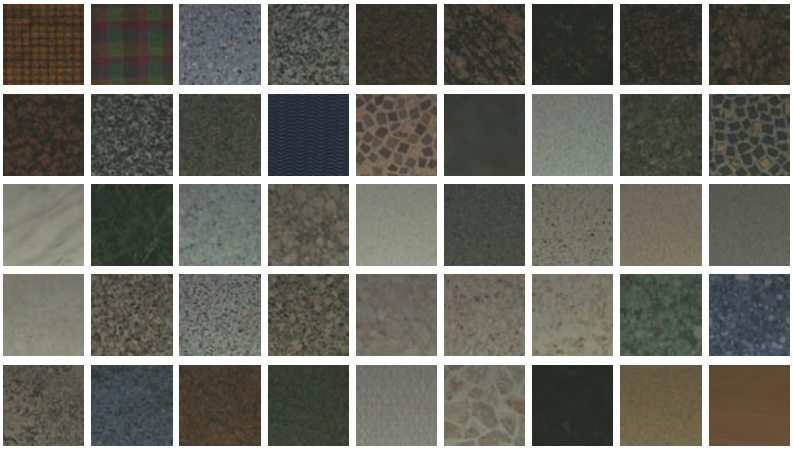

Fig. 8. Dataset A: 45 texture classes (one image for each class) from OuTex. *Canvas*{005, 021}; *Carpet*{005}; *Granite*{001, 003, 004, 005, 006, 007, 008, 009, 010}; *Paper*{006}; *Plastic*{001, 002, 003, 004, 005, 009, 016, 017, 018, 019, 020, 021, 022, 023, 024, 025, 026, 027, 028, 029, 030, 031, 032, 033, 034, 035, 036, 038, 040, 041}; *Wood*{006, 008}

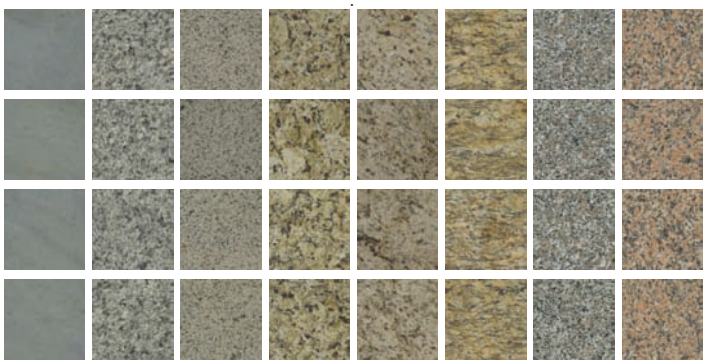

Fig. 9. Dataset B: 8 granite texture classes (four images for each class) from Mondial Marmi. From left to right: *Acquamarina*, *Azul Platino*, *Bianco Cristal*, *Giallo Napoletano*, *Giallo Ornamentale*, *Giallo Santa Cecilia*, *Rosa Beta*, *Rosa Porriño*

The second dataset, herein referred to as the dataset B (fig. 9), is composed of 8 granite texture classes (four images for each class). The image acquisition system is composed of a commercial digital camera (Samsung S850) and a Monster DOME Light 18.25 illuminator. We used the camera in manual mode with f-stop = 7.4 and exposure time = 1/30 s. The size of the original images is 1024 x 768 pixels. As in the dataset A, only the central part of each image is retained, resulting in a dimension of 544 x 544 pixels after cropping. Each image is subdivided into 4 non-overlapping sub-images, giving a database of 128 texture samples (16 for each class).

4.2. *Classification and error estimation procedure*

Texture classification is based on the nearest neighbour rule with the 'Manhattan' ($L1$) distance. Classification error has been evaluated by split-half validation with stratified sampling (Steyerberg et al., 2001): the texture samples were divided randomly into two non-overlapping groups (*training set* and *validation set*) of half the samples each. In order to assess robustness against rotation, the *training set* is always composed of textures from the 0° group, while the *validation set* is composed of rotated textures taken from the θ degrees group, with $\theta \in \{0°, 5°, 10°, 15°, 30°, 45°, 60°, 75°, 90°\}$. The percentage of correct classification is the ratio between the number of textures of the validation set correctly classified and the total number of textures of the validation set. For each angle the estimated percentage of correct classification is averaged over 100 different random partitions of data into training and validation set in order to make the estimation stable.

4.3. *Calibration of the input devices*

As discussed in section 3, characterization of the input device is needed both to compute the RGB values from R'G'B' (*inverse gamma correction*) and to move from a device-dependent space to a device-independent one (*colour calibration*). The calibration procedures described here below are based on the data provided by the *x-rite ColorChecker*® (fig. 10). It consists of 24 colour patches, each one representing common natural colours such as human skin, foliage, sky, additive and subtractive primaries and a six step grayscale. The x-rite ColorChecker has been

used in many applications (Grana et al., 2004; Haeghen et al., 2000; Martínez et al., 2007). Device independent colour values (sRGB and CIELAB) of each patch are provided together with the ColorChecker.

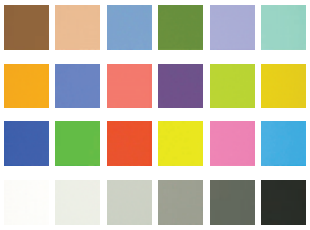

Fig. 10. The 24 colour patches of the *x-rite ColorChecker*®.

4.3.1. *Inverse gamma correction*

As a first step we estimate the parameters a, b and γ of each channel (equation 1). To estimate these parameters we considered the normalized values of the device-independent lightness ($\bar{L} = L/100$) of each patch and the corresponding device-dependent normalized response ($\bar{S_c} = S_c/255$) of each channel. For each channel $c \in \{1, 2, 3\}$ we seek the values that best fits equation 1, which means solving the following minimization problem:

$$\underset{(a_c, b_c, \gamma_c)}{argmin} \left\{ \sum_{i=1}^{N_\gamma} \left[\bar{S_c} - (a_c \bar{L_i}^{\gamma_c} + b_c) \right]^2 \right\} \tag{9}$$

where N_γ is the number of colour patches used in the procedure. Here we used the six grayscale patches of the ColorChecker, and thus $N_\gamma = 6$. Inverse gamma calibration is not needed in dataset A, since the OuTex imaging device does not adopt gamma correction (Mäenpää and Pietikäinen, 2004).

Conversely the images of the dataset B have been acquired with a commercial camera, and we experimentally verified that this camera does employ gamma correction. With the above described procedure we obtained the calibration data shown in table 2:

Table 2
Estimated value for gamma correction of dataset B

Channel	a	b	γ
R	1.0476	-0.11099	0.93937
G	1.0859	-0.13424	0.89653
B	1.0074	-0.10428	0.97102

4.3.2. *Colour calibration*

Colour calibration consists in determining the a_{ij} values which model the linear transform between RGB and sRGB spaces (eqn. 5). We considered all the 24 colour patches of the x-rite ColourChecker. Provided that we know, for each patch, the corresponding RGB and sRGB values, this gives $24 \times 3 = 72$ equations. The problem is overconstrained, so the unknowns can be estimated through a least-square procedure:

$$\mathbf{A} = \underset{(\mathbf{A}')}{argmin} \left\{ \sum_{c=1}^{N_c} \| \mathbf{sP}_c - \mathbf{A}'\mathbf{P}_c \|^2 \right\} \tag{10}$$

where A is the matrix defined in equation 5, $\mathbf{sP}_c = [sR_c\ sG_c\ sB_c]^T$, $\mathbf{P}_c = [R_c\ G_c\ B_c]^T$ and $N_c = 24$.

In dataset A we do not have at our own disposal the imaging system used to capture texture images. Nonetheless, since the spectra of the ColourChecker patches are available (Pascale, 2006), and both the spectral sensitivity of the camera and the spectrum of the illuminant are also available from the OuTex website [2], it is possible to estimate the device-dependent RGB values of the colour patches. Solving equation 10 we obtained the following transform for dataset A:

$$\begin{pmatrix} sR \\ sG \\ sB \end{pmatrix} = \begin{bmatrix} 1.9588 & -0.7808 & 0.4873 \\ 0.2406 & 1.2387 & 0.2931 \\ 0.2908 & -0.4375 & 1.9077 \end{bmatrix} \begin{pmatrix} R \\ G \\ B \end{pmatrix} \tag{11}$$

In dataset B the patches of the ColorChecker were acquired using the apparatus described in 4.1 under the same settings used to capture the granite textures. The R'G'B' output of the camera was inverse gamma-corrected to obtain the RGB values. Here it follows the resulting transform for dataset B:

$$\begin{pmatrix} sR \\ sG \\ sB \end{pmatrix} = \begin{bmatrix} 0.9736 & 0.0369 & -0.0576 \\ -0.0456 & 1.0139 & -0.0153 \\ 0.0462 & 0.0987 & 0.8041 \end{bmatrix} \begin{pmatrix} R \\ G \\ B \end{pmatrix} \tag{12}$$

5. Results and discussion

Tables 3 and 4 gather the classification results obtained with datasets A and B respectively. The tables are organized as follows: *feature space* indicates the features employed to model texture (see table 1); N denotes the number of colours of the palette; columns from 0° to 90° contain the percentage of correct classification obtained when the rotation angle of the textures of the test set varies from 0° to 90°; *mean* indicates the mean classification accuracy over the nine rotation angles considered. For comparison purpose we report at the top of both tables the results obtained with the grayscale CCR and LBP operators ($CCR_{3\times3}$ and $LBP_{3\times3}$) and their rotation-invariant-versions ($CCR^{ri}_{8,1}$, $CCR^{riu2}_{8,1}$, $LBP^{ri}_{8,1}$ and $LBP^{riu2}_{8,1}$).

The results confirm that the methods presented here are rotation-invariant, since there is little variation in the percentage of correct classification as the rotation angle of the test textures changes from 0° to 90°. The improvement in robustness against rotation becomes noticeable if we compare the results of the rotation-invariant multilayer CCR

[2] http://www.outex.oulu.fi/index.php?page=image_acquisition

Table 3
Classification results with dataset A (generic textures from OuTex).

Feature space	Colour space	N	Mean	0°	5°	10°	15°	30°	45°	60°	75°	90°
$CCR_{3\times3}$	GRAY	256	*52.63*	62.08	61.41	61.58	61.55	55.48	46.34	42.75	41.84	40.67
$CCR^{ri}_{8,1}$		256	*56.55*	56.82	55.17	54.59	56.42	55.46	57.98	56.29	58,14	58.08
$CCR^{riu2}_{8,1}$		256	*57.07*	57.04	55.75	54.83	56.95	56.11	58.79	57.21	58.29	58.65
$LBP_{3\times3}$	GRAY	256	*61.99*	78.79	78.69	78.67	76.70	66.84	52.38	44.16	41.12	40.58
$LBP^{ri}_{8,1}$		256	*70.88*	70.76	70.53	69.34	70.63	72.41	71.30	71.79	71.98	69.19
$LBP^{riu2}_{8,1}$		256	*70.46*	70.56	70.69	68.78	69.95	71.38	71.11	71.26	72.03	68.43
$ML\_CCR^{ri}_{8,1}$	RGB	8	*25.46*	26.44	26.21	24.26	23.17	25.45	26.11	25.31	27.44	24.78
$ML\_CCR^{ri}_{8,1}$		27	*70.17*	70.45	69.10	69.09	69.28	70.56	70.61	71.01	70.65	70.74
$ML\_CCR^{ri}_{8,1}$		64	*84.83*	86.34	86.04	84.29	83.33	85.53	84.00	85.77	85.46	82.71
$ML\_CCR^{riu2}_{8,1}$		8	*25.45*	26.43	26.23	24.19	23.23	25.46	26.08	25.40	27.24	24.81
$ML\_CCR^{riu2}_{8,1}$		27	*70.22*	70.51	69.14	68.94	69.21	70.86	70.75	71.21	70.61	70.79
$ML\_CCR^{riu2}_{8,1}$		64	*84.76*	86.29	86.00	84.32	83.36	85.45	83.89	85.71	85.49	82.37
$ML\_CCR^{ri}_{8,1}$	HSV	8	*43.28*	47.94	47.20	45.70	44.03	43.62	41.34	41.15	40.71	37.80
$ML\_CCR^{ri}_{8,1}$		27	*77.23*	77.40	78.60	77.44	77.03	78.58	76.77	76.99	76.60	75.70
$ML\_CCR^{ri}_{8,1}$		64	*88.06*	89.28	88.73	89.27	88.29	89.81	88.06	87.88	86.67	84.60
$ML\_CCR^{riu2}_{8,1}$		8	*43.46*	48.21	47.35	45.95	44.09	43.67	41.55	41.72	40.81	37.79
$ML\_CCR^{riu2}_{8,1}$		27	*77.43*	77.57	78.78	77.55	77.28	79.10	76.95	77.18	76.57	75.90
$ML\_CCR^{riu2}_{8,1}$		64	*88.07*	89.29	88.82	89.34	88.41	89.82	87.97	87.80	86.67	84.47
$ML\_CCR^{ri}_{8,1}$	sRGB	8	*73.21*	72.95	73.03	72.15	71.84	73.88	74.83	73.04	74.13	73.08
$ML\_CCR^{ri}_{8,1}$		27	*89.59*	90.70	90.11	89.73	89.80	90.18	89.61	89.62	88.91	87.62
$ML\_CCR^{ri}_{8,1}$		64	*91.09*	91.72	90.97	91.44	90.79	91.01	91.52	91.44	90.75	90.18
$ML\_CCR^{riu2}_{8,1}$		8	*73.32*	73.05	72.94	72.21	71.78	74.20	75.03	73.26	74.25	73.19
$ML\_CCR^{riu2}_{8,1}$		27	*89.65*	90.81	90.04	89.66	89.78	90.34	89.84	89.86	88.99	87.52
$ML\_CCR^{riu2}_{8,1}$		64	*91.03*	91.77	90.87	91.25	90.75	90.97	91.51	91.48	90.67	90.03
$ML\_CCR^{ri}_{8,1}$	sHSV	8	*70.92*	71.67	71.19	70.01	69.36	71.79	71.00	71.13	71.49	70.63
$ML\_CCR^{ri}_{8,1}$		27	*93.62*	94.81	94.28	94.49	93.97	94.02	94.30	93.40	92.50	90.86
$ML\_CCR^{ri}_{8,1}$		64	*94.98*	95.77	95.50	95.53	95.40	95.61	95.62	94.94	93.68	92.82
$ML\_CCR^{riu2}_{8,1}$		8	*71.15*	72.01	71.42	70.15	69.61	72.04	71.12	71.31	71.64	71.01
$ML\_CCR^{riu2}_{8,1}$		27	*93.67*	94.88	94.36	94.48	94.04	94.03	94.21	93.58	92.57	90.88
$ML\_CCR^{riu2}_{8,1}$		64	*94.92*	95.63	95.59	95.56	95.27	95.48	95.59	94.90	93.61	92.62
$ML\_CCR^{ri}_{8,1}$	CIELAB	8	*69.50*	67.44	68.89	68.32	69.44	70.16	70.91	71.46	70.16	68.75
$ML\_CCR^{ri}_{8,1}$		27	*86.93*	87.17	87.08	86.38	85.64	87.63	87.88	87.71	87.20	85.68
$ML\_CCR^{ri}_{8,1}$		64	*91.27*	92.12	91.22	91.22	91.20	91.80	91.46	91.88	90.63	89.90
$ML\_CCR^{riu2}_{8,1}$		8	*69.79*	67.75	69.13	68.53	69.48	70.44	71.21	71.88	70.65	69.09
$ML\_CCR^{riu2}_{8,1}$		27	*87.18*	87.35	87.19	86.47	85.98	88.02	88,15	87.99	87.55	85.88
$ML\_CCR^{riu2}_{8,1}$		64	*91.21*	91.95	91.23	91.27	91.08	91.70	91.36	91.84	90.54	89.93

features with those obtained with the $CCR_{3\times3}$. Another interesting outcome is that there is little difference between the $CCR^{ri}_{8,1}$ and the $CCR^{riu2}_{8,1}$ operators. These results are in agreement with those obtained with the LBP (Ojala et al., 2002a). This suggests that the increase in dimensionality associated to the multilayer approach can be compensated by using the uniform patterns.

Regarding to the role of colour, it clearly emerges from tables 3 and 4 that adding colour information markedly increases classification accuracy in both datasets. The number of colours of the palette has an important effect on classification. We found that, as the number of colours increases, the percentage of correct classification also increases, as one would expect. This effect is more evident in dataset A. The classification accuracy is also influenced by the space in which colour is represented. From both tables it comes out that, on average, device-independent spaces outperform device-dependent spaces. To explain this phenomenon we can consider, as an example, a texture image taken from the dataset A (fig. 11). Due to the specific adjustements of the acquisition system, the colour content of the image tend to spread over a limited portion of the RGB cube (fig. 11, left). This is a common characteristic of all the images of dataset A. As a consequence, uniform quantiza-

Table 4
Classification results with dataset B (granite textures).

Feature space	Colour space	N	Mean	0°	5°	10°	15°	30°	45°	60°	75°	90°
$CCR_{3\times3}$	GRAY	256	*85,54*	93,19	94,17	93,09	91,03	83,98	74,81	77,09	81,25	81,22
$CCR^{ri}_{8,1}$		256	*88,88*	87,63	86,20	86,95	86,03	87,83	88,81	91,91	92,00	92,52
$CCR^{riu2}_{8,1}$		256	*89,52*	88,34	86,44	87,53	87,00	89,06	89,23	92,22	92,44	93,45
$LBP_{3\times3}$	GRAY	256	*78,12*	97,09	96,03	96,13	94,39	69,38	58,27	59,81	64,64	67,38
$LBP^{ri}_{8,1}$		256	*89,72*	92,22	90,59	91,94	90,03	86,61	84,78	90,11	90,14	91,05
$LBP^{riu2}_{8,1}$		256	*88,90*	92,34	88,67	89,06	88,92	84,72	86,22	90,72	90,02	89,42
$ML\_CCR^{ri}_{8,1}$	RGB	8	*97.65*	96.88	96.80	98.08	97.91	97.28	97.53	97.67	98.72	97.98
$ML\_CCR^{ri}_{8,1}$		27	*98.88*	98,17	98.41	98.97	99.13	98.84	99.22	99.11	99.23	98.88
$ML\_CCR^{ri}_{8,1}$		64	*99.36*	99.28	98.81	99.17	99.58	99.52	99.47	99.47	99.47	99.47
$ML\_CCR^{riu2}_{8,1}$		8	*97.69*	96.97	96.89	98,19	98,13	97.27	97.58	97.58	98.56	98.08
$ML\_CCR^{riu2}_{8,1}$		27	*98.94*	98.28	98.56	98.98	99.17	98.86	99.22	99.17	99.27	98.97
$ML\_CCR^{riu2}_{8,1}$		64	*99.35*	99.20	98.81	99.17	99.59	99.52	99.47	99.48	99.45	99.45
$ML\_CCR^{ri}_{8,1}$	HSV	8	*97.75*	96.91	97.02	98.08	98.30	98.08	96.28	98.27	98.31	98.50
$ML\_CCR^{ri}_{8,1}$		27	*98.29*	97.63	97.92	98.92	98.33	97.92	97.50	98.78	98.48	99.11
$ML\_CCR^{ri}_{8,1}$		64	*98.74*	98,17	98.22	98.84	99.19	99.13	98.48	98.48	99.23	98.94
$ML\_CCR^{riu2}_{8,1}$		8	*97.76*	96.94	97.00	98.08	98.30	98.09	96.25	98.34	98.31	98.53
$ML\_CCR^{riu2}_{8,1}$		27	*98.29*	97.63	97.97	98.92	98.31	97.92	97.50	98.78	98.48	99.11
$ML\_CCR^{riu2}_{8,1}$		64	*98.78*	98.27	98.31	98.84	99.19	99.14	98.48	98.63	99.23	98.94
$ML\_CCR^{ri}_{8,1}$	sRGB	8	*98.08*	97.33	97.41	98.67	98.63	97.92	97.95	97.80	98.84	98,16
$ML\_CCR^{ri}_{8,1}$		27	*99.11*	98.55	98.72	99.09	99.17	99.39	99.38	99.31	99.34	99.05
$ML\_CCR^{ri}_{8,1}$		64	*99.16*	98.69	98.72	99.03	99.30	99.41	99.25	99.38	99.36	99.36
$ML\_CCR^{riu2}_{8,1}$		8	*98,14*	97.56	97.58	98.67	98.73	97.91	97.98	97.91	98.78	98,13
$ML\_CCR^{riu2}_{8,1}$		27	*99.16*	98.63	98.66	99.19	99.28	99.41	99.38	99.36	99.36	99.17
$ML\_CCR^{riu2}_{8,1}$		64	*99.16*	98.59	98.72	99.06	99.27	99.42	99.30	99.38	99.36	99.38
$ML\_CCR^{ri}_{8,1}$	sHSV	8	*98,12*	97.08	97.06	98.39	99.03	98.64	97.38	98.53	98.47	98.52
$ML\_CCR^{ri}_{8,1}$		27	*99.38*	99.05	99.53	99.75	99.80	99.03	98.78	99.19	99.69	99.56
$ML\_CCR^{ri}_{8,1}$		64	*99.84*	99.88	99.81	99.84	100.00	99.98	99.78	99.33	99.97	99.94
$ML\_CCR^{riu2}_{8,1}$		8	*98,17*	97.11	97.14	98.64	99.09	98.63	97.39	98.53	98.47	98.55
$ML\_CCR^{riu2}_{8,1}$		27	*99.40*	99.14	99.53	99.75	99.80	99.09	98.78	99.19	99.70	99.64
$ML\_CCR^{riu2}_{8,1}$		64	*99.85*	99.88	99.81	99.84	100.00	99.98	99.86	99.33	99.97	99.95
$ML\_CCR^{ri}_{8,1}$	CIELAB	8	*95.80*	95.98	94.95	96.33	95.39	93.84	95.06	96.17	97.63	96.86
$ML\_CCR^{ri}_{8,1}$		27	*99.80*	99.75	99.77	99.84	99.86	99.91	99.67	99.95	99.97	99.50
$ML\_CCR^{ri}_{8,1}$		64	*99.72*	99.64	99.69	99.66	99.89	99.72	99.63	99.67	99.67	99.91
$ML\_CCR^{riu2}_{8,1}$		8	*95.65*	95.48	94.72	96.33	94.91	93.91	95.19	96.06	97.66	96.56
$ML\_CCR^{riu2}_{8,1}$		27	*99.80*	99.75	99.77	99.83	99.86	99.91	99.66	99.95	99.97	99.52
$ML\_CCR^{riu2}_{8,1}$		64	*99.70*	99.61	99.67	99.66	99.89	99.70	99.59	99.67	99.64	99.91

tion of the colour space may be inadequate, since many different colours can be assigned the same index, while many entries of the palette are not used at all. Conversely colour calibration eliminates this bias, and colour spreads more uniformly over the colour space (fig. 11, right). Therefore a higher number of colours of the palette take part to colour indexing, which results in better separation bewteen the texture classes and improved classification accuracy.

It is widely accepted that texture descriptors that incorporate colour and texture into a single model are sensitive to changes in illumination, since the colour stimulus itself is intrinsically dependent on illumination. Although there is an extensive literature on the problem of robustness against illumination variation of colour attributes (colour constancy) this topic is still an open issue in computer vision. The approach presented in this paper relies on the assumption that illumination is kept constant, and both textures datasets used in the experimental activity satisfy this condition. In presence of varying illumination conditions the colour calibration procedure described in section 4.3.2 can be used as a pre-processing stage to compensate for variance in illumination and changes in spectral sensitivity of the camera.

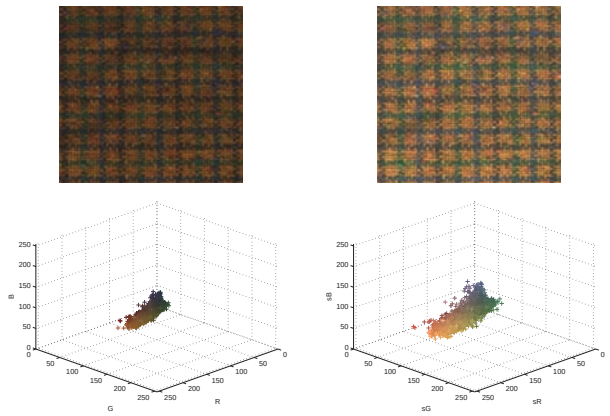

Fig. 11. From left to right: texture *canvas005* and its colour distribution before colour calibration (RGB space) and after colour calibration (sRGB space).

6. Conclusions

In this paper we presented an improved version of the *Coordinated Clusters Representation* (CCR) for rotation-invariant classification of colour textures. Rotation invariance is achieved by using uniform circular patterns, following an approach similar to the one proposed for the LBP. Colour and texture are combined into a single model through colour indexing and the multilayer approach. The experimental results make evident that classification is not affected by relative rotation between training end test images. The results also show that considering colour and texture jointly provides a marked improvement of the classification accuracy in comparison with the grayscale CCR and LBP features. An important advantage of the method presented here is that, differently from the original CCR, it does not rely on previous binarization of the texture image. Our results show that classification accuracy depends on the colour space, and that device-independent colour spaces perform better.

Acknowledgements

This work was partially supported by the *Fondazione CARIT* (Terni, Italy) under the project entitled "*Sviluppo di metodologie di simulazione del comportamento di materiali impiegati nell'edilizia e nell'industria meccanica*", and by the *Xunta de Galicia* (Spain) under the grant *PGIDIT04REM303003PR*. The authors thank *Mondial Marmi* SpA (Perugia, Italy), for having provided them with the granite tiles used in the experiments.

The remarks and suggestions made by the anonymous reviewers are gratefully acknowledged.

References

Arvis, V., Debain, C., Berducat, M., Benassi, A., 2004. Generalization of the cooccurrence matrix for colour images: application to colour texture classification. Image Analysis and Stereology 23, 63–72.

Bianconi, F., Fernández, A., González, E., Ribas, F., 2007. Texture classification through combination of sequential colour texture classifiers. Lecture Notes in Computer Science 4756, 235–243.

Boukouvalas, C., De Natale, F., De Toni, G., Kittler, J., Marik, R., Mirmehdi, M., Petrou, M., Le Roy, P., Salgari, R., and Vernazza, G. ,1998. ASSIST: Automatic system for surface inspection and sorting of tiles. Journal of Materials Processing Technology, 82(1-3):179–188.

Chindaro, S., Sirlantzis, K., Deravi, F., 2005. Texture classification system using colour space fusion. Electronics Letters 41, 589–590.

Drimbarean, A., Whelan, P., 2001. Experiments in colour texture analysis. Pattern Recognition Letters 22, 1161–1167.

Funt, B., Finlayson, G., 1995. Color constant color indexing. IEEE Transactions on Pattern Analysis and Machine Intelligence 17, 522–528.

Grana, C., Pellacani, G., Seidenari, S., Cucchiara, R., 2004. Color calibration for a dermatological video camera system. In: Proceedings of the 17th International Conference on Pattern Recognition, Cambridge (UK), Vol. 3. pp. 798–801.

Haeghen, Y., Naeyaert, J., Lemahieu, I., Philips, W., 2000. An imaging system with calibrated color image acquisition for use in dermatology. IEEE Transactions on Medical Imaging 19, 722–730.

Hauta-Kasari, M., Parkkinen, J., Jaaskelainen, T., Lenz, R., 1996 Generalized cooccurrence matrix for multispectral texture analysis. In: Proceedings of the 13th International Conference on Pattern Recognition, Wien (Austria), Vol 2., pp. 785-789.

Hiremath, P., Shivashankar, S., Pujari, J., 2006. Wavelet based features for color texture classification with application to CBIR. International Journal of Computer Science and Network Security 6, 124–133.

Huang, J., Kumar, S.R., Mitra, M., Zhu, W., Zabih, R. 1997. Image Indexing Using Color Correlograms. In: Proceedings of the IEEE Conference on Computer Vision and Pattern Recognition, San Juan (Puerto Rico), pp. 762-768.

Jain, A., Healey, G., 1998. A multiscale representation including opponent color features for texture recognition. IEEE Transactions on Image Processing 7, 124–128.

Kang, H., 2006. Computational Color Technology. Spie Press.

Kurmyshev, E., Sánchez-Yañez, R., 2005. Comparative experiment with colour texture classifiers using the CCR feature space. Pattern Recognition Letters 26, 1346–1353.

Kurmyshev, E., Cervantes, M., 1996. A quasi-statistical approach to digital binary image representation. Revista Mexicana de Física, 42(1), 104-116.

Kurmyshev, E., Poterasu, M., Guillen-Bonilla, J., 2007. Image scale determination for optimal texture classification

using Coordinated Clusters Representation. Applied Optics 46, 1467–1476.

Lepistö, L., Kunttu, I., Visa, A., 2005. Rock image classification using color features in Gabor space. Journal of Electronic Imaging 14(4), 040503.

Manthalkar, R., Biswas, P. K., Chatterji, B. N., 2002. Rotation invariant color texture classification in perceptually uniform color spaces. In: Proceedings of the III Indian Conference on Computer Vision, Graphics and Image Processing (in CD-ROM), Ahmedabad (India).

Martínez, L., Arbiol, R., Palà, V., Pérez, F., 2007. Digital metric camera radiometric and colorimetric calibration with simultaneous CASI imagery to a CIE standard observer based colour space. In: Proceedings of the IEEE International Geoscience and Remote Sensing Symposium, Barcelona (Spain), pp. 4140-4143.

Mäenpää, T., Pietikäinen, M., 2004. Classification with color and texture: jointly or separately? Pattern Recognition 37.

Mäenpää, T., Pietikäinen, M., 2005. Texture analysis with Local Binary Patterns. In: Handbook of Pattern Recognition and Computer Vision, C.H. Chen and P.S.P. Wang eds., World Scientific Publishing, pp. 197-216.

Ojala, T., Pietikäinen, M., Mäenpää, T., 2002a. Multiresolution gray-scale and rotation invariant texture classification with Local Binary Patterns. IEEE Transactions on Pattern Analysis and Machine Intelligence 24, 971–987.

Ojala, T., Pietikäinen, M., Mäenpää, T., Viertola, J., Kyllönen, J., Huovinen, S., 2002b. Outex - new framework for empirical evaluation of texture analysis algorithms. In: Proceedings of the 16th International Conference on Pattern Recognition, Quebec (Canada), Vol. 1, pp. 701-706.

Palm, C., 2004. Color texture classification by integrative co-occurrence matrices. Pattern Recognition 37, 965–976.

Panjwani, D. K., Healey, G., 1995. Markov random field models for unsupervised segmentation of textured color images. IEEE Transactions on Pattern Analysis and Machine Intelligence 17, 939–954.

Pascale, D., 2006 Colorchecker rgb and spectra. Available at: www.babelcolor.com/main_level/ColorChecker.htm.

Paschos, G., 2001. Perceptually uniform color spaces for color texture analysis: An empirical evaluation. IEEE transactions on Image Processing 10, 932–937.

Petrou, M., García Sevilla, P. G., 2006. Image Processing. Dealing with Texture. Wiley Interscience.

Pietikäinen, M., Mäenpää, T., Viertola, J., 2002. Color texture classification with color histograms and Local Binary Patterns. In: Proceedings of the 2nd International Workshop on Texture Analysis and Synthesis, Copenhagen (Denmark), pp. 109-112.

Sánchez-Yáñez, R. E., Kurmyshev, E., Cuevas, F., 2003. A framework for texture classification using the Coordinated Clusters Representation. Pattern Recognition Letters 24, 21–31.

Sánchez-Yáñez, R. E., Kurmyshev, E., Fernández, A., 2003. One-class texture classifier in the CCR feature space. Pattern Recognition Letters 24, 1503–1511.

Sertel, O., Lozanski, G., Shana'ah, A., Catalyurek, U., Saltz, J., Gurcan, S., 2008. Texture classification using nonlinear color quantization: application to histopathological image analysis. In: Proceedings of the IEEE International Conference on Acoustics, Speech and Image Processing, Las Vegas (USA), pp. 597-600.

Singh, M., Markou, M., Singh, S., 2002. Colour Image Texture Analysis: Dependence on Colour Spaces. In: Proceedings of the 16th International Conference on Pattern Recognition, Quebec (Canada), pp. 672-675.

Song, K., Kittler, J., Petrou, M., 1996. Defect detection in random colour texture. Image Vision and Computing 14, 667–683.

Steyerberg, E., Harrell, F., Borsboom, G., Eijkemans, M., Vergouwe, Y., Habbema, J., 2001. Internal validation of predictive models: Efficiency of some procedures for logistic regression analysis. Journal of Clinical Epidemiology 54, 774–781.

Van den Broek, E. V., Rikxoort, E. V., 2004. Evaluation of color representation for texture analysis. In: Proceedings of the 16th Belgium-Netherlands Conference on Artificial Intelligence, Nijmegen (Holland), pp. 51-58.

Van de Wouver, G., Scheunders, P., Livens, S., Van Dyck, D. 1999. Wavelet correlation signatures for color texture characterization. Pattern Recognition 32(3), 443–451.

Vhrel, M., Trussell, H., 1998. The mathematics of color calibration. In: Proceedings of the International Conference on Image Processing. Vol. 1. Chicago (USA), pp. 181–185.

Wyszecki, G., Styles, W., 1982. Color Science. Concepts and Methods, Quantitative Data and Formulae. Second Edition. Wiley-Interscience.